ON A CONSERVATIVE SOLUTION TO CHECKERBOARDING: EXAMINING THE CAUSES OF NON-PHYSICAL PRESSURE MODES

***J.A. Hopman*[1], *À. Alsalti-Baldellou*[1,2], *F.X. Trias*[1] *and J. Rigola*[1]**

[1] ***Heat and Mass Transfer Technological Center, Technical University of Catalonia***
ESEIAAT, c/Colom 11, 08222 Terrassa, Spain
[2] ***Termo Fluids SL, Sabadell (Barcelona), Spain; www.termofluids.com***

jannes.hopman@upc.edu, github.com/janneshopman

Abstract

In computational fluid dynamics (CFD), the checkerboard problem remains a challenging issue when employing collocated grid arrangements for complex geometries. It manifests as oscillatory and non-physical pressure modes, which can disrupt fluid motion and compromise numerical accuracy. In this study, a closer look is taken at the mathematical origins of checkerboarding and a self-regulating solution to mitigate its adverse effects is proposed. Through an analysis of the Navier-Stokes equations discretized using a fractional step method, we identify three key mechanisms that lead to checkerboarding: the use of a pressure predictor, the choice of Poisson solver, and inconsistent interpolators. To quantify checkerboarding, the checkerboarding coefficient is introduced, a non-dimensional measure that accounts for field decoupling on arbitrary meshes. A Taylor-Green vortex and a lid-driven cavity case were used to test the proposed solution. By introducing a self-regulating parameter, a balance between reduced checkerboarding and minimal numerical dissipation was achieved. The results indicate the effectiveness of this approach, which exhibits stable behavior while maintaining accuracy in the selected cases.

1 Introduction

CFD codes used in industrial applications often deal with complex geometries and benefit from employing a collocated grid arrangement. To discretise the divergence and gradient operators of the Navier-Stokes equations in such cases, a central differencing scheme is commonly used. However, this results in a wide-stencil Laplacian, where neighbouring odd and even cells become decoupled, leading to the formation of oscillatory and non-physical patterns. These patterns remain unnoticed by the CFD algorithm as they lie within the kernel of the discrete Laplacian. This issue is referred to as the checkerboard problem [Ferziger et al. (1996)].

To address the oscillation problem, many collocated CFD methods use a compact-stencil Laplacian, which couples neighboring cells. However, this approach introduces numerical dissipation [Rhie and Chow (1983); Felten and Lund (2006)], disrupting fluid motion, particularly at small turbulent length scales [Verstappen and Veldman (2003)]. Alternatively, a non-dissipative solution involves filtering out the spurious pressure modes that reside within the kernel of the wide-stencil Laplacian [Shashank et al. (2010); Hopman et al. (2022)]. Nevertheless, this method may not be feasible for complex geometries due to the computational expense of calculating the kernel. Even when utilizing the compact-stencil Laplacian, oscillatory patterns may still manifest, especially with small timesteps in unsteady scenarios [Felten and Lund (2006)] or when incorporating a predictor pressure in the velocity predictor [Komen et al. (2021)].

This has led to the question how the checkerboard problem arises in the first place, and how it can arise even without the use of the wide-stencil Laplacian. In this work, an analysis of the most probable mathematical origins of the problem is given. To measure the occurrence of the problem, a suitable quantification method is derived, even for complex geometries. Subsequently, a Taylor-Green vortex case and a lid-driven cavity case are used to test the methods to provoke and quantify checkerboarding. Finally, a solution to the problem is tested which is low-dissipative and absent of checkerboarding.

2 Mathematical origins of checkerboarding

To examine the mathematical origins of checkerboarding, the Navier-Stokes equations were discretised and a fractional step method (FSM) was used, for advancement in time. This method is given by algorithm 1, in which Forward Euler time integration is used as an example, for simplicity. θ_p controls the pressure predictor and is usually set to 0 or 1, corresponding to the classical FSM or the Van Kan method, respectively [Van Kan (1986)]. The notation of algo-

$$R_c^n = \mathbf{u}_c^n - \Delta t \Omega^{-1} \left(C\left(\mathbf{u}_s^n\right) + D \right) \mathbf{u}_c^n \quad \text{(A1.1)}$$

$$\mathbf{u}_c^p = R_c^n - G_c \theta_p \tilde{\mathbf{p}}_c^n \quad \text{(A1.2)}$$

$$L\tilde{\mathbf{p}}_c' = M_c \mathbf{u}_c^p = M_c R^n - L_c \theta_p \tilde{\mathbf{p}}_c^n \quad \text{(A1.3)}$$

$$\mathbf{u}_c^{n+1} = \mathbf{u}_c^p - G_c \tilde{\mathbf{p}}_c' \quad \text{(A1.4)}$$

$$\mathbf{u}_s^{n+1} = \Gamma_{cs} \mathbf{u}_c^p - G\tilde{\mathbf{p}}_c' \quad \text{(A1.5)}$$

$$\tilde{\mathbf{p}}_c^{n+1} = \theta_p \tilde{\mathbf{p}}_c^n + \tilde{\mathbf{p}}_c' \quad \text{(A1.6)}$$

Algorithm 1: Fractional step method including pressure predictor. Forward Euler is used as an example for simplicity.

rithm 1 follows the work of [Trias et al. (2014)], where

$$L = MG, \quad (1)$$

$$L_c = M_c G_c = M\Gamma_{cs}\Gamma_{sc} G, \quad (2)$$

$$\Gamma_{sc} = \Omega^{-1}\Gamma_{cs}^T \Omega_s, \quad (3)$$

$$-M^T = \Omega_s G, \quad (4)$$

$$-M_c^T = -(M\Gamma_{cs})^T = \Omega\Gamma_{sc} G = \Omega G_c, \quad (5)$$

with Laplacian, L, gradient, G, divergence, M, collocated operators denoted by subscript c, cell-to-face interpolator, Γ_{cs}, face-to-cell interpolator, Γ_{sc}, cell volumes, Ω and face volumes, Ω_s. Note that the Laplacians are symmetric and that L_c and G_c have kernels that contain spurious modes. Below, an analysis is given of the possible origins of the checkerboard problem.

Mechanism 1. When using $\theta_p = 0$ so that there is effectively no pressure predictor and letting $\Delta t \to 0^+$, the second term on the RHS of equation (A1.1) diminishes until $\mathbf{u}_c^p = \mathbf{u}_c^n$, which leads to:

$$\mathbf{u}_c^n = \mathbf{u}_c^{n-1} - G_c \tilde{\mathbf{p}}_c^n = \mathbf{u}_c^0 - G_c \sum_i^n \tilde{\mathbf{p}}_c^i \quad (6)$$

$$L\tilde{\mathbf{p}}_c^{n+1} = M_c \mathbf{u}_c^0 - L_c \sum_i^n \tilde{\mathbf{p}}_c^i \quad (7)$$

$$L\check{\mathbf{p}}_c^{n+1} = M_c \mathbf{u}_c^0 + (L - L_c)\,\check{\mathbf{p}}_c^n \quad (8)$$

in which $\check{\mathbf{p}}_c^n = \sum_i^n \tilde{\mathbf{p}}_c^i$. This is similar to solving the wide-stencil Poisson equation through a stationary iterative method. Therefore, effectively, the pressure field gives a solution for L_c, even though a compact-stencil Laplacian is used. A way to accelerate this effect even further is by using $\theta_p = 1$, which causes a larger part of the pressure field to be multiplied by the wide-stencil Laplacian, seen on the RHS of equation (A1.3).

Mechanism 2. The second method involves the choice of Poisson solver. For a stationary iterative method and the compact-stencil Laplacian, the Poisson equation is solved as:

$$\begin{aligned}\tilde{\mathbf{p}}_c' = &\sum_{i=0}^{k} \left(I - \bar{L}^{-1}L\right)^i \bar{L}^{-1} M_c \mathbf{u}_c^p \\ &+ \left(I - \bar{L}^{-1}L\right)^{k+1} \tilde{\mathbf{p}}_c'^{(n-1)}\end{aligned} \quad (9)$$

where $\bar{L}$ is a computationally cheaply invertible part of L, after splitting the matrix as: $L = \bar{L} + \hat{L}$, e.g. $\bar{L} = diag(L)$ for the Jacobian method. The second term on the RHS of equation (9) accounts for the initial guess and is used to reduce the number of necessary iterations. If the image of $\bar{L}^{-1}$, Im $\left(\bar{L}^{-1}\right)$, is non-orthogonal to the kernel of L_c, Ker (L_c), the solution can contain checkerboard modes. These modes can subsequently be preserved by the implementation of the initial guess. Similarly, if a preconditioner based on incomplete factorisations is used as:

$$Q_L^{-1} L Q_R^{-1} \tilde{\mathbf{q}}_c^{n+1} = Q_L^{-1} M_c \mathbf{u}_c^p \quad (10)$$

where $Q_R^{-1}\tilde{\mathbf{q}}_c^{n+1} = \tilde{\mathbf{p}}_c^{n+1}$, then Im $\left(Q_R^{-1}\right)$ might not be orthogonal to Ker (L_c), possibly leading to checkerboarding.

Mechanism 3. The third method involves the wide-stencil Laplacian that is implicitly formed by the collocated divergence and gradient, M_c and G_c, on the RHS of equations (A1.3) and (A1.4). If both interpolations in these operators are consistent, e.g. both midpoint, the operator is symmetric and the image and kernel are orthogonal, i.e. $L_c^T = L_c \to$ Im $(L_c) \perp$Ker (L_c). If not, the result of this operation can contain checkerboard modes. This implicit $M_c G_c$ occurs when rewriting RHS of equation (A1.3) using equations (A1.1), (A1.2) and (A1.4):

$$\begin{aligned}M_c \mathbf{u}_c^p = &M_c R^{n-1} - (1+\theta_p) M_c G_c \tilde{\mathbf{p}}_c^n \\ &- \Delta t M_c \Omega^{-1} \left(C\left(u_s^n\right) + D \right) \mathbf{u}_c^n.\end{aligned} \quad (11)$$

Therefore, checkerboarding might arise if the interpolators in G_c and M_c are chosen to be inconsistent with respect to each other, i.e. not according to equation (3).

From these mechanisms, it was found that checkerboarding was most easily provoked using $\theta_p = 1$ and subsequently retained by using an initial guess in the iterative solver, as seen in the second term of the RHS of equation (9). In simple laminar cases, letting $\Delta t \to 0^+$ did not consistently provoke a qualitatively significant level of checkerboarding. The use of a preconditioner led to similar levels of checkerboarding as the results without the use of any preconditioner. And finally, inconsistencies in the interpolators of the M_c and G_c operators either led to insignificant levels of checkerboarding or immediate instability where the solution diverged.

3 Quantification method

If checkerboarding is quantified purely as the modes of pressure that lie on the kernel of L_c, then the spurious pressure modes are determined by the mesh.

It was shown by [Hopman et al. (2022)] that in this case, the modes could only exist on Cartesian meshes, or could be easily removed by slightly adjusting any mesh so that there are no more spurious modes on the kernel of L_c. Furthermore, such a definition does not include any pressure fields that show the decoupling only in some parts of the domain. Therefore, a definition is needed that can quantify the decoupling seen in checkerboarding on arbitrary meshes and will also include fields with only local decoupling.

To arrive to such a definition, it is useful to first consider the pressure error that is often introduced to resolve the problem. The pressure diffusion energy budget term, which should globally equal zero, is given by $-\mathbf{u}_c^{n+1}\Omega G_c\tilde{\mathbf{p}}_c^{n+1}$. In methods like algorithm 1 it is non-zero due to the divergence of the collocated velocity field, given by:

$$M\mathbf{u}_s^{n+1} = M\left(\Gamma_{cs}\mathbf{u}_c^p - G\tilde{\mathbf{p}}_c'\right) = \mathbf{0}_c, \tag{12}$$

$$\begin{aligned} M_c\mathbf{u}_c^{n+1} &= M\left(\Gamma_{cs}\mathbf{u}_c^p - \Gamma_{cs}\Gamma_{sc}G\tilde{\mathbf{p}}_c'\right) \\ &= M\left(G - \Gamma_{cs}\Gamma_{sc}G\right)\tilde{\mathbf{p}}_c' \\ &= \left(L - L_c\right)\tilde{\mathbf{p}}_c'. \end{aligned} \tag{13}$$

Using equation (5), the pressure diffusion budget is rewritten as:

$$\begin{aligned} -\mathbf{u}_c^{n+1}\Omega G_c\tilde{\mathbf{p}}_c^{n+1} &= \tilde{\mathbf{p}}_c^{n+1^T} M_c\mathbf{u}_c^{n+1} \\ &= \tilde{\mathbf{p}}_c^{n+1^T}\left(L_c - L\right)\tilde{\mathbf{p}}_c' \end{aligned} \tag{14}$$

To make this term independent of temporal integration method, any dependency on time and θ_p should be removed. Moreover, since adding a constant pressure to any solution should not change this term, the calculation is done after removing the volume-weighted average pressure from the field, as: $\mathbf{P}_c = \mathbf{p}_c - \mathbf{p}_c^T\Omega\mathbf{1}_c/\left(\mathbf{1}_c^T\Omega\mathbf{1}_c\right)$, and $\mathbf{1}_c$ is the one-vector. Furthermore, dependency on the norm of the pressure field should be removed, this is done by dividing out $||\mathbf{P}_c|| = \mathbf{P}_c\Omega\mathbf{P}_c$ Finally, to make the term non-dimensional, a non-dimensional gradient operator is introduced, G^*, which is a cell-to-face incidence matrix. So that:

$$[G^*\mathbf{P}_c]_f = [\delta_{n,f}G\mathbf{P}_c]_f = \mathbf{P}_{c,n} - \mathbf{P}_{c,o}, \tag{15}$$

$$M^* = -G^{*^T}\Omega_s, \tag{16}$$

$$L^* = M^*G^* = -G^{*^T}\Omega_s G^*, \tag{17}$$

$$L_c^* = M_c^*G_c^* = -G_c^*\Omega G_c^*. \tag{18}$$

Finally, the time-independent non-dimensional quantification for checkerboarding is then given by the checkerboarding coefficient:

$$\begin{aligned} C_{cb} &= \frac{\mathbf{P}_c^T\left(L_c^* - L^*\right)\mathbf{P}_c}{\mathbf{P}_c^T\Omega\mathbf{P}_c} \\ &= \left(||G^*\mathbf{P}_c|| - ||G_c^*\mathbf{P}_c||\right)/||\mathbf{P}_c|| \end{aligned} \tag{19}$$

This term has the nice intuitive quality that the difference in the numerator is larger for fields with a bigger component lying on the kernel of G_c^*, which is desirable to measure fields with checkerboarding.

Using C_{cb}, a proper evaluation of checkerboarding can be done and an examination of the origins of the problem can be made. To do so, a Taylor-Green vortex and a lid-driven cavity case were run using $\theta_p = 0$ and $\theta_p = 1$, while measuring C_{cb}. Since the value of θ_p directly provokes checkerboarding, another value of θ_p was introduced, that regulates θ_p through negative feedback: $\theta_p = \frac{1}{1+C_{cb}}$. In the absence of checkerboarding, this coefficient will tend to 1, and it will deminish to 0 if the levels of checkerboarding increase. The resulting three solvers are denoted as follows:

Solver	θ_0	θ_1	θ_{cb}
θ_p	0	1	$\frac{1}{1+C_{cb}}$

4 Results

The Taylor-Green vortex case was used to examine numerical dissipation of the solvers, since it is expected that θ_0 shows less checkerboarding at the cost of being more dissipative. Furthermore, the checkerboarding coefficient, C_{cb}, was monitored over time. This case consists of four two-dimensional vortices on a square domain with periodic boundaries. The initial velocity and pressure fields are given by continuous functions and their decay, which depends on the viscosity, also have analytical solutions. The analytical velocity and pressure fields over time are given by:

$$[\mathbf{u}_{c,Ana}]_i = \begin{pmatrix} \sin(x_i)\cos(y_i)e^{-2\nu t} \\ -\cos(y_i)\sin(y_i)e^{-2\nu t} \end{pmatrix}, \tag{20}$$

$$[\mathbf{p}_{c,Ana}]_i = \frac{1}{4}\big(\cos(2x_i) + \cos(2y_i)\big), \tag{21}$$

from which the analytical kinetic energy over time is taken as $E_{k,Ana} = ||\mathbf{u}_{c,Ana}||$.

The case was run on a $2\pi \times 2\pi$ domain on a Cartesian uniform 33×33 mesh. The symmetry-preserving Runge-Kutta OpenFOAM solver ***RKSymFoam*** was used, which was developped for [Komen et al. (2021)] and can be found in the GitHub repository given in the author's affiliations. This solver was modified to include θ_{cb}. The Runge-Kutta 3 method was used for temporal integration with $\Delta t = 0.01$ and the case was run with $\nu = \{0, 0.01\}$. The results for the loss of kinetic energy can be seen in figures 1 and 2. The effects of θ are clearly visible, with θ_0 seemingly most dissipative. C_{cb} remained constant and very low for all cases around $C_{cb} \approx 0.005$, meaning θ_{cb} was able to stay close to 1, hence giving similar results to θ_1.

The lid-driven cavity case consists of a two-dimensional $L \times L$ square box, where the top wall is moving to the right with velocity U_L. The case was run with $L = 1$ on a 33×33 uniform Cartesian mesh, with $U_L = 1$ and $\nu = 0.01$, leading to a Reynolds

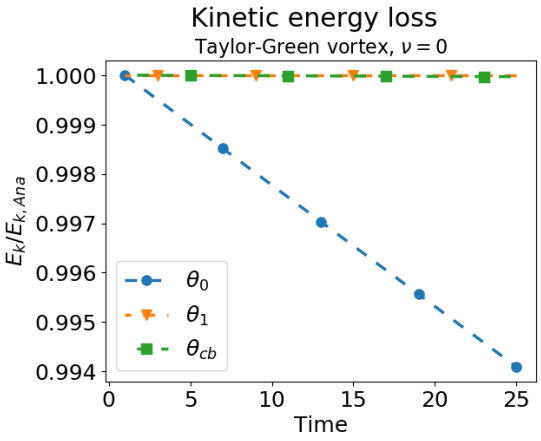

Figure 1: Numerical dissipation of each solver. θ_1 and θ_{cb} show conservation of kinetic energy, whereas θ_0 shows numerical dissipation.

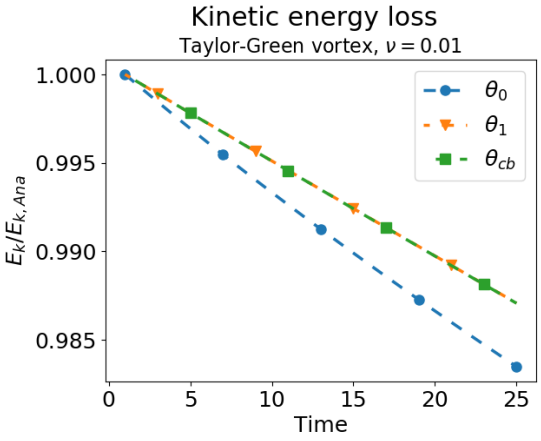

Figure 2: Numerical dissipation of each solver. All solvers show numerical dissipation relative to the analytical solution, with θ_0 showing this strongest.

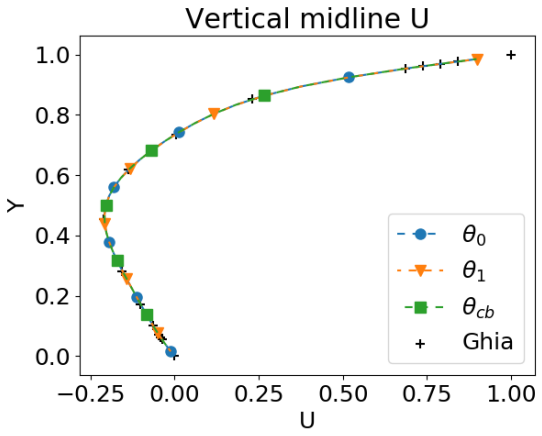

Figure 3: Horizontal velocity, U, on the vertical midline ($x = 0.5$), compared to results of [Ghia et al. (1982)]

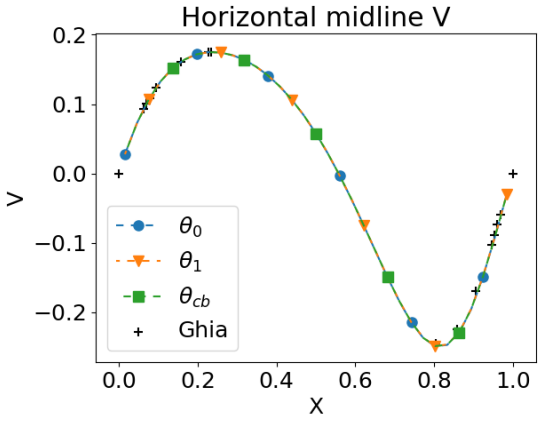

Figure 4: Vertical velocity, V, on the horizontal midline ($y = 0.5$), compared to results of [Ghia et al. (1982)]

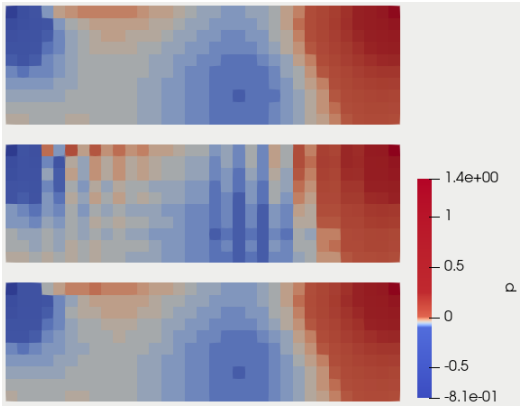

Figure 5: Pressure field near the lid for θ_0 (top), θ_1 (center) and θ_{cb} (bottom)

number of $Re = U_L L/\nu = 100$. *RKSymFoam* was used with the Runge-Kutta 3 method and $\Delta t = 0.01$. Figures 3 and 4 show close agreement to the results of [Ghia et al. (1982)].

In figure 5 parts of the resulting pressure fields for each solver can be seen to give a qualitative impression of the checkerboard problem. Checkerboarding patterns can clearly be seen in θ_{cb} compared to the other solvers. This confirms that the checkerboard problem can originate through the inclusion of a pressure predictor. Interestingly, θ_{cb} does not show checkerboarding, suggesting that the value was adjusted as a result of the arising checkerboarding, thereby self-regulating its damping. The results for the velocity profiles in figures 3 and 4 show no negative impact from this damping, whereas the resulting pressure field is qualitatively greatly improved.

From figure 6 these findings are confirmed by the quantification through C_{cb}. Initially C_{cb} rises while the field is establishing, once a stable solution is reached, the levels of checkerboarding do not change.

θ_{cb} nicely balances between θ_0 and θ_1 indicating that the self-regulation works properly and the stabilized value of $C_{cb} = 0.20$ indicates that $\theta = 1/(1 + 0.2) = 0.83$ is a proper value for this case.

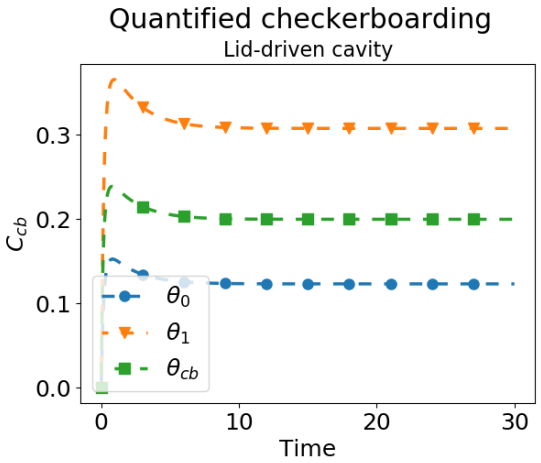

Figure 6: Checkerboard coefficient C_{cb} over time showing that θ_{cb} balances between the checkerboard-prone θ_1 and the more dissipative θ_0

Finally, a closer look at the pressure in the cells adjacent to the lid is given in figure 7. From this figure the spurious behaviour close to the lid can clearly be seen. Additionally, the solution field for θ_{cb} was filtered from pressure modes that lie on the kernel of L_c, which was done by projecting the pressure field onto the kernel modes and subtracting the result from the original field [Shashank et al. (2010); Hopman et al. (2022)]. This method is restricted to Cartesian and other well-structured meshes, for which the kernel modes can be easily calculated. The filtered solution is indicated with the markers in figure 7. It can be seen that filtering slightly improves the result, however it is not by any means enough to solve the checkerboard problem.

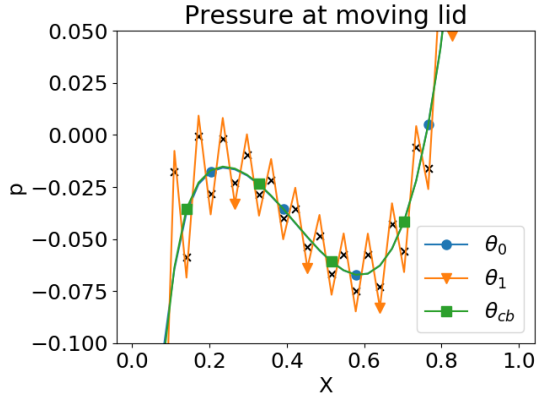

Figure 7: Spurious pressure fields at the nodes adjacent to the lid can only be seen for θ_1, even after filtering (indicated by $\times$)

5 Conclusions

The main mechanisms of the origins of checkerboarding were identified to be through the use of a pressure predictor, through the solver and through inconsistent interpolators. In this work, a focus was put on recreating the problem through the pressure predictor, since it was easiest to reproduce, even in small academic cases. In future work, the other mechanisms will be analysed even further by experimenting with larger scale turbulent cases, to see if their effect is more prevalent in those situations. The modes that were provoked in this work were shown to also include pressure modes that lie outside of the kernel of L_c. The filtering method through projection onto the kernel therefore is not sufficient to solve the problem, neither is it feasible on complex geometries. The checkerboarding coefficient that was derived in this work showed to properly quantify the problem. Its robustness on other, more challenging cases will be tested in future work. The development of a new solver through the use of an adjustable pressure predictor coefficient, that self-regulates through negative feedback from the checkerboarding coefficient, showed promising results. However, this solution is limited to solving checkerboarding caused by a pressure predictor, it has yet to be tested if it can resolve checkerboarding caused by other effects. This solver will also be tested on other cases and could prove to be a low-dissipative, checkerboard-free solver for collocated grid arrangements.

Acknowledgments

This work is supported by the FusionCAT project (001-P-001722) co-financed by the European Union Regional Development Fund within the framework of the ERDF Operational Program of Catalonia 2014-2020 with a grant of 50% of total cost eligible and the RETOtwin project (PDC2021-120970-I00) of *Ministerio de Economía y Competitividad*, Spain. J.A.H. is supported by the predoctoral grant FI 2022 (2022 FI_B1 00204) of the *Catalan Agency for Management of University and Research Grants (AGAUR)*. Àdel Alsalti Baldellou has also been supported by the predoctoral grants DIN2018-010061 and 2019-DI-90, given by MCIN/AEI/10.13039/501100011033 and the Catalan Agency for Management of University and Research Grants (AGAUR), respectively.

References

Felten, F.N. and T.S. Lund (2006). "Kinetic energy conservation issues associated with the collocated mesh scheme for incompressible flow". In: *Journal of Computational Physics* 215(2), pp. 465–484.

Ferziger, J.H., M. Perić, and R.L. Street (1996). *Computational methods for fluid dynamics*. springer.

Ghia, U.K.N.G., K.N. Ghia, and C.T. Shin (1982). "High-Re solutions for incompressible flow using the Navier-Stokes equations and a multigrid

method". In: *Journal of computational physics* 48(3), pp. 387–411.

Hopman, J.A., F.X. Trias, and J. Rigola (2022). "On a Conservative Solution to Checkerboarding: Examining the Discrete Laplacian Kernel Using Mesh Connectivity". In: *DLES13, 13th ERCOFTAC Workshop on Direct and Large Eddy Simulation: 26-28 October 2022, Udine, Italy*. ERCOFTAC.

Komen, E.M.J., J.A. Hopman, E.M.A. Frederix, F.X. Trias, and R.W.C.P. Verstappen (2021). "A symmetry-preserving second-order time-accurate PISO-based method". In: *Computers & Fluids* 225, p. 104979.

Rhie, C.M. and W.L. Chow (1983). "Numerical study of the turbulent flow past an airfoil with trailing edge separation". In: *AIAA journal* 21(11), pp. 1525–1532.

Shashank, J. Larsson, and G. Iaccarino (2010). "A collocated incompressible Navier-Stokes solver with exact mass, momentum and kinetic energy conservation in the inviscid limit". In: *Journal of Computational Physics* 229(12), pp. 4425–4430.

Trias, F.X., O. Lehmkuhl, A. Oliva, C.D. Pérez-Segarra, and R.W.C.P. Verstappen (2014). "Symmetry-preserving discretization of Navier–Stokes equations on collocated unstructured grids". In: *Journal of Computational Physics* 258, pp. 246–267.

Van Kan, J.J.I.M. (1986). "A second-order accurate pressure-correction scheme for viscous incompressible flow". In: *SIAM journal on scientific and statistical computing* 7(3), pp. 870–891.

Verstappen, R.W.C.P. and A.E.P. Veldman (2003). "Symmetry-preserving discretization of turbulent flow". In: *Journal of Computational Physics* 187(1), pp. 343–368.